Applied Catalysis A, General 602 (2020) 117698

Contents lists available at ScienceDirect

Applied Catalysis A, General

journal homepage: www.elsevier.com/locate/apcata

Efficient and green electrochemical synthesis of 4-aminophenol using porous Au micropillars

Maxime Tranchant[a], Albert Serrà[a,*], Christopher Gunderson[a], Enrico Bertero[a], Jaume García-Amorós[b,c], Elvira Gómez[c,d], Johann Michler[a], Laetitia Philippe[a]

[a] Empa, Swiss Federal Laboratories for Materials Science and Technology, Laboratory for Mechanics of Materials and Nanostructures, Feuerwerkerstrasse 39, CH-3602 Thun, Switzerland

[b] Grup de Materials Orgànics, Departament de Química Inorgànica i Orgànica (Secció de Química Orgànica), Universitat de Barcelona, Martí i Franquès, 1, E-08028 Barcelona, Catalonia, Spain

[c] Grup d'Electrodeposició de Capes Primes i Nanoestructures (GE-CPN), Departament de Ciència de Materials i Química Física, Universitat de Barcelona, Martí i Franquès, 1, E-08028, Barcelona, Catalonia, Spain

[d] Institute of Nanoscience and Nanotechnology (IN^{2}UB), Universitat de Barcelona, Barcelona, Catalonia, Spain

ARTICLE INFO

Keywords:
Shape-controlled electrodeposition
SU-8 molds
Colloidal crystal lithography
Electrosynthesis
4-aminophenol

ABSTRACT

The development of new, efficient, chemoselective, and seemingly stable catalysts to rapidly convert 4-nitrophenol into 4-aminophenol, which is a particularly valuable chemical within multiple industries, is highly required. The use of non-toxic and non-corrosive chemicals for 4-aminophenol synthesis presents further challenges. We show a simple and scalable shape-controlled electrodeposition using a dual-template method for the synthesis of well-defined porous Au micropillar array electrodes to enhance electrocatalyst stability, efficiency, and durability during the electroreduction of 4-nitrophenol. Consequently, we avoid the use of toxic and aggressive chemical reducing agents and minimize the production of residues. Surface areas up to 55.2 $m^2 g^{-1}$ are achieved, which represent a substantial improvement over non-architectured Au film electrodes. Porous Au micropillars exhibit excellent yields (100 %), chemoselectivity (other byproducts are not detected), and a high kinetic constant of 2.5×10^{-2} min^{-1}, which is impressively higher than those reported recently for Au thin films or Au-based electrocatalysts.

1. Introduction

4-aminophenol is an important chemical within multiple industries. It is a developer in the photography industry and is an intermediate in the pharmaceutical and dye industry [1–3]. For instance, it serves as an intermediate not only in the synthesis of paracetamol, a medication used worldwide that appears on the World Health Organization's list of essential medicines [4,5], but also in the manufacture of sulfur and azo dyes, which have important applicability in the textile, leather, and alimentary industries [6].

The chemical reduction of 4-nitrophenol to 4-aminophenol by sodium borohydride is considered a model reaction for metal nanoparticles due to its well-studied kinetics and associated color changes [7,8]. Two routes for the synthesis of 4-aminophenol are the hydrogenation of nitrobenzene [9,10], or the nitration of phenol followed by the chemical reduction of the resulting 4-nitrophenol by sodium borohydride although other reducing agents such as hydrazine have been used as well [11–13]. However, these methods require the addition of toxic reagents as opposed to an electrosynthetic route that allows for direct control over the movement of electrons. A reactant can be converted into a desired product by precisely controlling the potential and current, thereby eliminating extra-toxic reagents typically found in organic synthesis [14]. Organic electrosynthesis is performed primarily in aqueous solution, not in organic solvents, which minimizes the production of residues as well as allows important reductions in energy and resource consumption [15,16].Electrosynthetic reactions can be further tuned by introducing a proper electrocatalyst or by employing an indirect electrosynthesis mechanism [17]. However, the electrode surface can become contaminated and passivated during the course of the synthesis. Additionally, the reaction is confined to the electrode surface or near it, resulting in longer synthesis times, although this can be compensated for by using electrodes with more surface area [18,19].

A precursor to 4-aminophenol, 4-nitrophenol is a significant water pollutant identified by the United States Environmental Protection

* Corresponding author.
E-mail address: albert.serraramos@empa.ch (A. Serrà).

https://doi.org/10.1016/j.apcata.2020.117698
Received 25 April 2020; Received in revised form 2 June 2020; Accepted 13 June 2020
Available online 19 June 2020

Agency, which finds its way into water supplies because of chemical plant discharge and as the byproduct of the degradation of pesticides from agricultural runoff [20,21]. Previous methods employed for the degradation of 4-nitrophenol in wastewater have been the photocatalysis of water splitting by a semiconductor such as zinc oxide or titanium dioxide [22–24]. The process works through the generation of hydroxyl radicals that then chemically oxidize 4-nitrophenol in solution [25]. Importantly, 4-nitrophenol is a redox-active molecule and numerous materials have been shown to be capable of electrochemically detecting it, such as graphene oxide, gold, platinum, or bismuth [26–30]. The electrooxidation of 4-nitrophenol into ammonia and carbon dioxide has been demonstrated on boron-doped diamond electrodes previously [31]. Studies focused on the electrooxidation of 4-nitrophenol showed that a simultaneous electroreduction of 4-nitrophenol occurs at their stainless steel cathode which, at a basic pH, produced a solid film of 4-aminophenol with no discernable intermediates or byproducts [32].

Here we present the direct electrochemical reduction of 4-nitrophenol into 4-aminophenol using a novel gold electrode. The electrode fabrication uses colloidal crystal templating to generate a nanoscale, three-dimensional template that is filled through gold electroplating. The colloidal crystal template is removed through plasma etching leaving an interconnected and nanoporous geometry with a roughness factor 25 times higher than that of a gold film electrode. The use of gold as the electrode material reduces the effect of hydrogen evolution when compared to platinum, which can lead to undesirable byproducts. Gold also increases the stability of the electrode against degradation, and the electrode is shown to be stable for multiple electroreduction cycles. The structural identity of the electrosynthesized product has been elucidated by means of ^{1}H nuclear magnetic resonance (NMR) spectroscopy, thereby revealing the successful formation of 4-nitrophenol, as expected. The transformation of 4-nitrophenol into 4-aminophenol has been monitored by means of high performance liquid chromatography (HPLC) and UV–vis spectroscopy. HPLC also confirmed that no by-products were generated during the electrolytic process. Thus, porous Au micropillars enable the quantitative, clean and ecofriendly transformation of 4-nitrophenol.

2. Experimental

2.1. Dual template electrosynthesis of well-defined porous gold micropillars

A novel ordered porous Au micropillar array electrode has been successfully fabricated by combining a dual templating method utilizing SU-8 molds and colloidal crystal lithography with galvanostatic electrodeposition. The multi-step process is described in detail below:

- **Fabrication of SU-8 molds**: Micromolds obtained by UV-LIGA technology (see Supporting information for details) were used as templates to produce Au electroplated micropillars. All preparation steps for the template fabrication were performed in a Class 10.000 cleanroom (Empa in Thun). The template design consisted of a matrix of hollow cylinders with an external diameter of 225 µm, an internal diameter of 25 µm and an interdistance of 50 µm between the patterns. Fig. 1a gives the dimensions of the molds and the corresponding array exposed on the wafer.
- **Colloidal crystal templating:** The SU-8 molds were then pretreated with an oxygen plasma during 12 min at 400 W and 450 mTorr (Muegge STP Compact, Muegge GmbH) to make the template hydrophilic and allow for good penetration of the colloidal suspension. The molds were then filled with deionized water (18.2 MΩ cm) by vacuum impregnation to remove the possibly trapped air. A commercially available colloidal suspension (Sigma-Aldrich) consisting of SiO_2 spheres (5 % w/w) with an average diameter of 500 ± 20 nm was used to create the crystal templates. 150 µL of suspension was poured onto the wetted substrate, and the sample was left in an oven at 55 °C until evaporation was completed. The ordering of the spheres occurred through the combined effect of gravity, attractive capillary forces due to surface tension effects, and convection induced by evaporation, forming colloidal crystals exhibiting a FCC structure [33–35]. The crystal templates were thereafter heated in an oven at 170 °C. This step would favor interconnections in the particle network and enhance the cohesion of the colloidal structure [36], thereby limiting the risk of disaggregation during the subsequent steps. Higher curing temperatures have been reported for SiO_2 spheres [37], but the glass transition temperature of cross-linked SU-8 requires the annealing temperature to be below 200 °C to safely prevent any structural changes in the micromolds [38–40]. A summary of the aforementioned colloidal crystal templating process is given in Fig. 1b.
- **Gold electrodeposition:** The dual templates previously produced were treated prior to electrodeposition with an oxygen plasma at 600 W for 6 min (PVA Tepla PlaTeG, PVA Industrial Vacuum Systems GmbH) to ensure a good penetration of the electrolyte inside the templates along with a uniform nucleation of Au, which would thereafter favor the formation of a continuous network [33]. Electrodeposition was carried out using a three-electrode setup with the previously prepared sample as a working electrode, a mixed metal oxide coated titanium anode (Platinode 187 SO, Umicore) as a counter electrode, and a saturated $Ag/AgCl/Cl^-$ electrode as a reference electrode. A potentiostat (PGSTAT 302 N, Metrohm Autolab B.V.) along with the NOVA software (version 2.1) was used to perform the deposition in galvanostatic mode at a current density of $-5\ mA\ cm^{-2}$ for 6 h.

Au was deposited from a commercially available aqueous cyanide based electrolyte (AURUNA 5500 EF, Umicore) containing 16 g L^{-1} of Au(I) in a volume of 500 mL. The pH of the bath was adjusted to 5.5 with citric acid ($C_6H_8O_7$) 2 M and ammonium hydroxide 28–30 %. Both $C_6H_8O_7$ and the ammonium hydroxide solution were supplied by Sigma-Aldrich. The process temperature was adjusted to 40 ± 1 °C using a temperature-controlled circulator (F12-ED, Julabo) coupled to a double walled cell for temperature control.

The obtained electrodeposited pillars were polished through a two-step process using an automatic polishing machine (M.M.8400, Lam Plan SA). A lapping plate and 6 µm sized diamond particles were first used to etch away the overgrowth. A polishing plate along with 3 µm sized diamond particles were then utilized to get a flat and smooth top surface. Diamond particles (Neodia Biodiamant) were supplied by Lam Plan SA as well. The photoresist along with SiO_2 nanoparticles were removed by plasma etching for 2 h at 400 W and a temperature of 60 °C. The process pressure was 450 mTorr and with gas flow rates of 875 sccm of O_2, 30 sccm of CF_4 and 50 sccm of N_2. The microstructure of the electrodeposited Au was separately investigated by electroplating a thin Au film onto an oxygen plasma pretreated (Muegge STP Compact, Muegge GmbH) Au/Cr/Si substrate without an SU-8 template. Deposition was carried out at -5 mA cm^{-2} during 70 min in direct current mode to reach a final thickness of approximately 20 µm.

2.2. Characterization of porous gold micropillars

The morphology of the micropillars was observed using a field-emission scanning electron microscope (FE-SEM, Hitachi S-4800,). The structural characterization was conducted with high-resolution X-ray diffraction using a Bruker D8 Discovery diffractometer in the Bragg-Brentano configuration with CuK_α radiation. Au (111) peak along with the Scherrer equation were used to estimate the grain size. The mass-normalized electrochemical active surface area (ECSA) and the roughness factor (RF, i.e. ratio between the ECSA value and the geometrical area of the electrode) values were calculated by integrating the charge associated with the reduction of Au oxide in the cyclic voltammograms recorded in 0.5 M sulfuric acid at the scan rate of 100 mV s^{-1}.

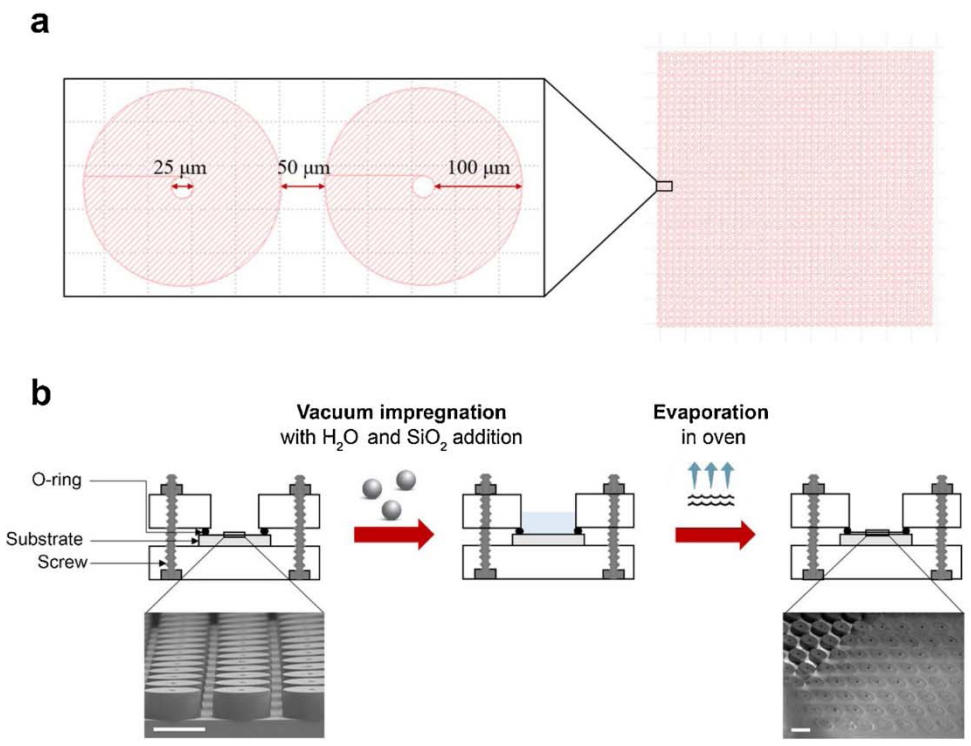

Fig. 1. (a) Schematic of a pillar geometry and the corresponding array. (b) Schematic of the colloidal crystal templating, with a cross-section view of the setup used for the process. Scale bar: 200 µm.

Electrochemical surface area was estimated assuming that the charge required to reduce superficial Au oxides was 390 µC cm^{-2} [41,42]. The electrochemical experiments were performed at 25 °C using a three-electrode electrochemical cell with our Au working electrode, a Pt wire counter electrode, and a Ag/AgCl/KCl (3 M)/Na_2SO_4 (0.5 M) reference electrode. In order to normalize the ECSA values, the total mass of Au was determined by using inductively coupled plasma mass spectroscopy (ICP-MS). Au electrodes were digested using a conventional digestion method with a mixture of hydrofluoric acid and nitric acid for ICP-MS analysis.

2.3. Electrosynthesis of 4-aminophenol

4-aminophenol was selectively electrosynthesized by potentiostatic electrocatalyzed reduction of 4-nitrophenol on Au-based electrodes from a 5 mM 4-nitrophenol and 0.4 M sodium sulphate (pH = 2, adjusted using dilute sulfuric acid) solution at 25 °C. Electrochemical experiments were carried out in a conventional three-electrode cell using an Autolab with PGSTAT 302 N (Metrohm Autolab B.V.) equipment and NOVA (version 2.1) software. Bare and porous Au micropillars electrodes were employed as electrocatalysts, and consequently, as working electrodes during the electrosynthesis of 4-aminophenol. The reference and counter electrodes were a Ag/AgCl/KCl (3 M)/Na_2SO_4 (0.5 M) and a Pt wire, respectively. Cyclic voltammetry (CV) was carried out at 25 °C at a scan rate of 100 mV s^{-1} in order to select the most adequate potential range for the electroreduction of 4-nitrophenol. The potentiostatic electroreduction of 4-nitrophenol was conducted also at 25 °C under magnetic stirring (400 rpm).

The electrocatalyzed reduction of 4-nitrophenol over Au-based electrodes was monitored by UV–vis spectroscopy and HPLC. Absorption spectra were recorded with a UV-1800 Shimadzu UV–vis spectrophotometer (Shimadzu Corporation). The kinetic progress of the electroreduction of 4-nitrophenol was tracked by measuring the time-dependent absorbance of 4-nitrophenoxide at 400 nm. HPLC chromatograms were recorded with a Waters 2795 Alliance HT Separations Module equipped with a Waters 2996 photodiode array detector. The HPLC instrument was coupled to a ZQ micromass 2000 mass spectrometer. The column used was an X-bridge Shield RP18 (particle size: 3.5 µm, internal diameter: 2.1 mm, length: 100 mm). The mobile phase flowed at 0.5 mL min^{-1}. The mobile phase used was a gradient from CH_3CN and H_2O 95:5 v/v (both containing a 0.1 % v/v of formic acid) to pure CH_3CN. This gradient was applied over a period of 9 min. HPLC solutions were prepared using Millipore-MilliQ water and acetonitrile of HPLC-MS grade (VWR-BDH Prolabo). The structural identity of the electrosynthesized product was confirmed by ^1H NMR spectroscopy. ^1H NMR (400 MHz) spectra were registered with a Varian Mercury spectrometer. ^1H NMR spectra were processed with the MestRec Nova software (version 10.0). NMR spectra were recorded in d_6-DMSO after liquid-liquid extraction. The catalyst stability and reusability was proved by measuring the electroreduction activity of 4-nitrophenol for 6 cycles under the same reaction conditions. After the six cycles, morphological analysis of Au-based electrodes and ECSA values were also determined.

3. Results and discussion

3.1. Electrosynthesis and characterization of porous gold micropillars

As described in Section 2.1, micropillar array molds with a 25 µm internal diameter were produced by UV lithography. The molds consisted of an 80 µm thick SU-8 photoresist coating on an Au-coated silicon wafer. Molds dimensions were chosen to obtain a final pillar aspect ratio in between 2 and 3. UV-LiGA molds were plasma pretreated, filled with deionized water, and thereafter with the colloidal suspension of monodisperse silicon dioxide spheres, left for evaporation, and finally cured in an oven.

A good filling of the molds with SiO_2 nanoparticles was achieved after sedimentation. As shown in Fig. S1, colloidal crystals exhibiting different sized grains with a hexagonal arrangement, in agreement with the (111) plane of the FCC structure, were obtained. The surface of the dual template after annealing highlights the presence of dislocations, as a result of internal stress buildup induced by the sedimentation profile

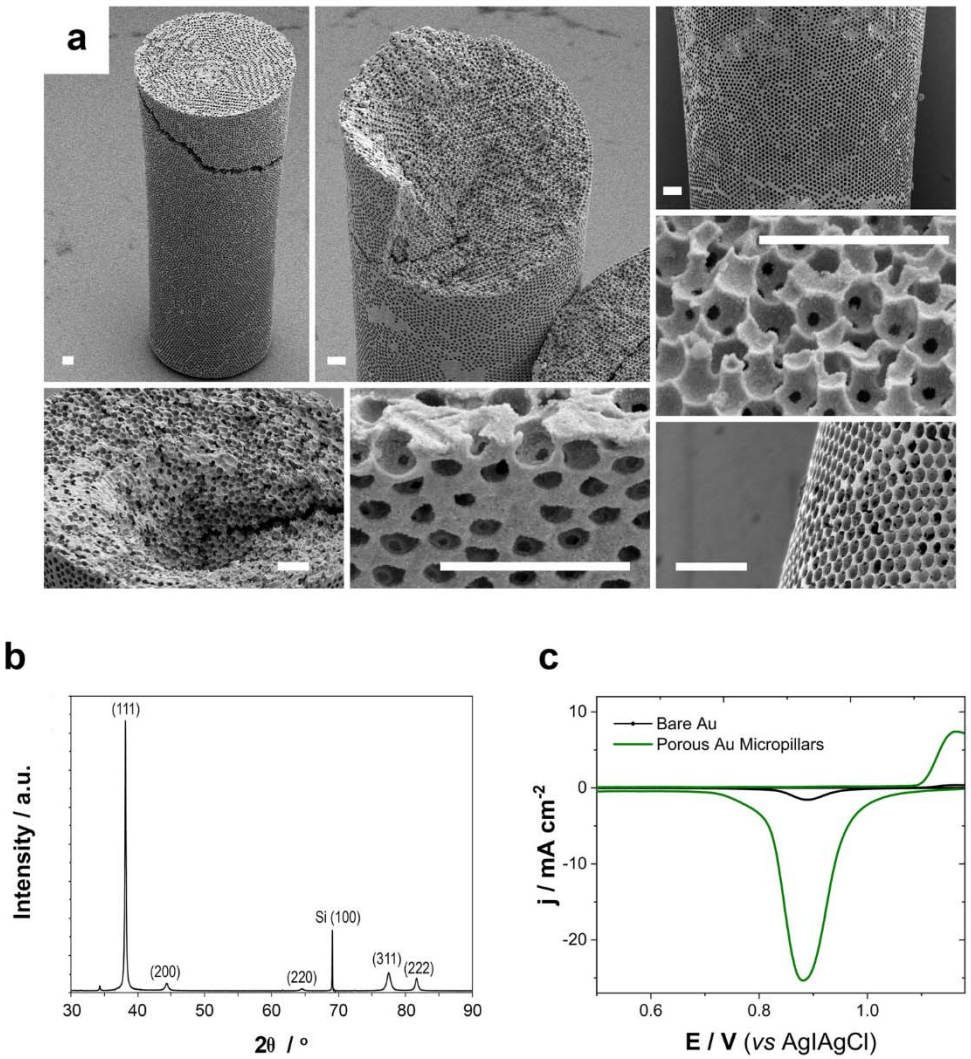

Fig. 2. (a) FE-SEM micrographs of porous Au micropillars. Scale bar: 2 µm. (b) XRD pattern of the Au thin film in the 30°–90° 2θ region. (c) Cyclic voltammetry (forty cycles) of bare Au and porous Au micropillars electrodes in H_2SO_4 0.5 M solutions at room temperature at a scan rate of 100 mV s^{-1}.

and the substrate's topography, along with vacancies, similar to those inherently present in a crystalline solid.

The dual template previously prepared was pretreated with oxygen plasma and vacuum impregnated with the Au electrolyte to ensure uniformity in the deposit. The deposition process was then performed in galvanostatic mode, at an optimized current density of $-5\,mA\,cm^{-2}$. Au micropillars were slightly overgrown after electrodeposition, resulting in caps visible on top of the UV-LiGA molds, as shown in Fig. S2. The sample was mechanically polished to get a flat and smooth top surface.

Fig. 2a shows SEM pictures of the nanocrystalline porous Au micropillars after the reactive ion etching step. The good uniformity of gold after electroplating confirms that a good filling of the molds as well as a good packing quality of the spheres prior to electrodeposition was achieved. A long-range ordering throughout the height as well as inside the pillar confirms this observation. It can thus be postulated that SiO_2 spheres did undergo plasma pretreatment and electroplating without any apparent significant change in their ordering. As clearly shown in Fig. 2a, the porosity is uniformly distributed over the entire surface with no visible non-porous region. Importantly, the average pore size of all the samples was maintained at around 500 nm, which is in good agreement with the average size of the SiO_2 nanoparticles, thereby indicating that the gold matrix was not subjected to any deformation mechanism affecting its final microstructure in the steps following electroplating.

The microstructural characterization was conducted from a thin Au film electroplated at the same current density of $-5\,mA\,cm^{-2}$ as was used for the micropillars preparation. The X-ray diffractogram plotted in Fig. 2b shows a clear (111) preferred texture of the film, with an average grain size of 42 nm as determined by the Debye-Scherrer equation assuming a shape factor of 0.9, in good agreement with previously reported works [5]. It is worth noticing that the 100 nm Au seed layer is expected to contribute to the intensity of the corresponding peak in the X-ray diffractogram as it covers all the wafer surface.

The mass-normalized ECSA and the RF values (Table 1) of porous Au micropillars were estimated from the CV that was recorded in a 0.5 M sulfuric acid solution with a scan rate of 100 mV s^{-1} (Fig. 2c). Au-based electrodes were scanned within the potential range corresponding to the formation of a superficial oxide layer (1.2 to 0.5 V). The

Table 1
Pore diameter, roughness factor and mass-normalized ECSA values of bare Au and porous Au micropillars electrodes.

	Pore diameter / nm	Roughness factor (RF)	ECSA / $cm^2\,mg^{-1}$
Bare Au	–	2.8	1.4
Porous Au micropillars	500 ± 30	70.5	55.2

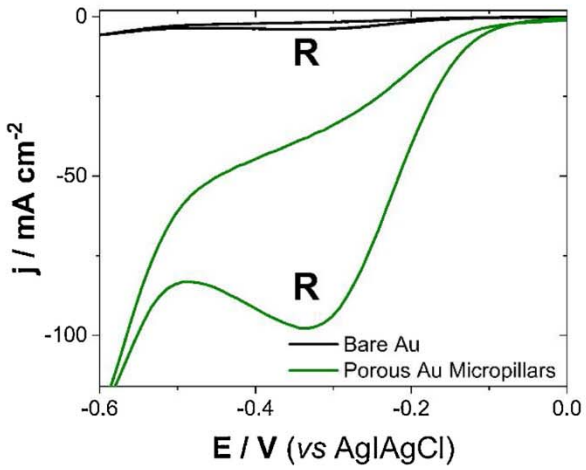

Fig. 3. Cyclic voltammograms under stationary conditions of 5 mM of 4-nitrophenol and 0.4 M of Na_2SO_4 (pH = 2) on bare Au and porous Au micropillar electrodes at a temperature of 25 °C and at a scan rate of 100 mVs^{-1}.

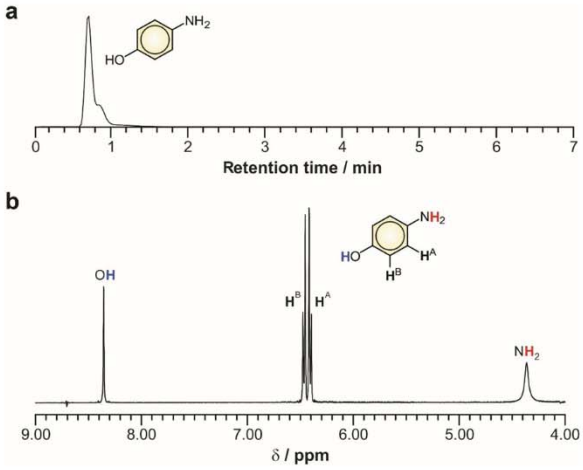

Fig. 4. (a) HPLC chromatogram of the electrolytic bath after 180 min and (b) ^{1}H NMR spectrum, recorded in d_6-DMSO, of the electrolytic bath extracted with diethyl ether.

charge density involved in the Au oxidation-reduction of porous Au micropillars demonstrates the important increase in effective and accessible areas of the micropillar array gold electrode per fixed geometrical area when compared with bare Au electrodes (approximately 25 times lower).

Consequently, porous Au micropillar array electrodes were effectively fabricated by a simple and scalable multi-step process based on dual template electrodeposition. The as-prepared porous micropillar electrodes possess well-defined and uniformly distributed pores, with high specific surface areas, which render them strong candidates for electrocatalytic applications compared to continuous films. Note that this approach can be extended to prepare more complex architectures. In general, it is important to note that Au electrodes are the most suitable electrocatalysts for 4-nitrophenol electroreduction, due to its high overpotential to hydrogen formation preventing significant hydrogen coevolution during 4-nitrophenol electroreduction which avoids the generation of undesired byproducts and extra power waste [43,44].

3.2. Electrosynthesis of 4-aminophenol

Fig. 3 depicts the cyclic voltammetry of the electrocatalyzed reduction of 4-nitrophenol (5 mM) on Au-based electrodes in 0.4 M of Na_2SO_4 (pH = 2) at a scan rate of 100 mVs^{-1}. The voltammograms were typically scanned from +0.0 to −0.6 V versus an Ag/AgCl/KCl (3 M)/Na_2SO_4 (0.5 M) reference electrode. In that range of potentials, a large reduction peak (R) was observed, attributed to the irreversible reduction of 4-nitrophenol to 4-hydroxyl aminophenol; no oxidation peaks were observed on the reverse sweep under these experimental conditions [44–50].

The high surface area promoted by porous Au micropillars compared with that of bare Au electrodes improved efficiency but did not shift the reduction potential in terms of porosity, especially mesoporosity, which could dramatically change the surface reactivity. Based on the results shown by cyclic voltammograms, a potential of −0.4 V versus an Ag/AgCl/KCl (3 M)/Na_2SO_4 (0.5 M) electrode was selected for the electrosynthesis of 4-aminophenol. The electrosynthesis of 4-aminophenol, under the selected conditions, was a mass transfer-controlled process. For this reason, the electroreduction was performed under magnetic stirring conditions (i.e., 400 rpm). Note that the porous size of the micropillar microstructures was approximately 500 nm, a size that was sufficiently large to consider that linear diffusion occurs inside the overall structure, i.e., it was unnecessary to take into consideration any possible spherical diffusion. Stationary reduction current values were recorded in the electrosynthesis process, and correspond to a limit current density (j_L).

The electrosynthesis of 4-aminophenol via the electroreduction of 4-nitrophenol proceeded in two stages; nitrophenol was selectively electroreduced to 4-hydroxyl aminophenol, after which a nucleophilic attack by water on the aromatic ring of 4-hydroxyl aminophenol formed 4-aminophenol. Using dilute sulfuric acid and adjusting the pH of the electrochemical media proved to be critical in the completion of the electrosynthesis of 4-aminophenol [49–53]. The HPLC chromatogram (Fig. 4a), recorded after 180 min of electrolysis, reveals that not only was 4-nitrophenol quantitatively converted into products but also that no parallel undesired reactions occurred during electrolysis. Indeed, a unique peak, with a retention time of 0.72 min, was detected in the corresponding HPLC chromatogram. Furthermore, the structural identity of the electrosynthesized product (4-aminophenol) was confirmed by means of ^{1}H NMR spectroscopy. For this purpose, the acidic electrolyzed solution was extracted with diethyl ether. Under these conditions, 4-nitrophenol was selectively transferred to the organic layer and isolated after distilling off the solvent under reduced pressure. As expected, the ^{1}H NMR spectrum of the residue, dissolved in d_6-DMSO, shows two doublet signals centered at 6.40 and 6.46 ppm (^3J = 8.8 Hz), belonging to H^A and H^B, respectively (Fig. 4b). In addition, two broad singlets peaking at 4.36 and 8.32 ppm are also observed, ascribable to the amino and phenol functions of the molecule, respectively.

To analyze the performance of porous Au micropillars, the potentiostatic electroreduction of 4-nitrophenol was achieved using bare Au and porous Au micropillar electrodes (Figs. 5 and S3). As expected, porous Au micropillars exhibited a significantly higher current density than the bare Au due to the former's higher effective surface area. The spectroscopic monitoring of the process was evaluated by measuring the temporal evolution of the absorbance of 4-nitrophenoxide at λ_{max} = 400 nm, taking advantage of the significant absorption of this species in the visible region of the electromagnetic spectrum in alkaline medium (Figs. 5a and S3b). The simultaneous appearance of an absorption band at 310 nm, ascribable to 4-aminophenoxide, is also observed. For those measurements, 40 µL of the reactant solution was diluted into 3 mL of 0.5 M NaOH in advance in order to record the UV–vis spectra. The color of the alkaline solutions also proved the electroreduction of 4-nitrophenol, as a change in color from yellowish to colorless was observed. The electroreduction of 4-nitrophenol when Au bare electrodes were used was significantly lower (i.e., yield of 19.4 % after 180 min of reaction) than with porous Au micropillars (i.e., yield of 99.0 % after 180 min of reaction), possibly due to the highly accessible surface area. The kinetics of the process was also evaluated chromatographically from the diminishment of the integrated area of

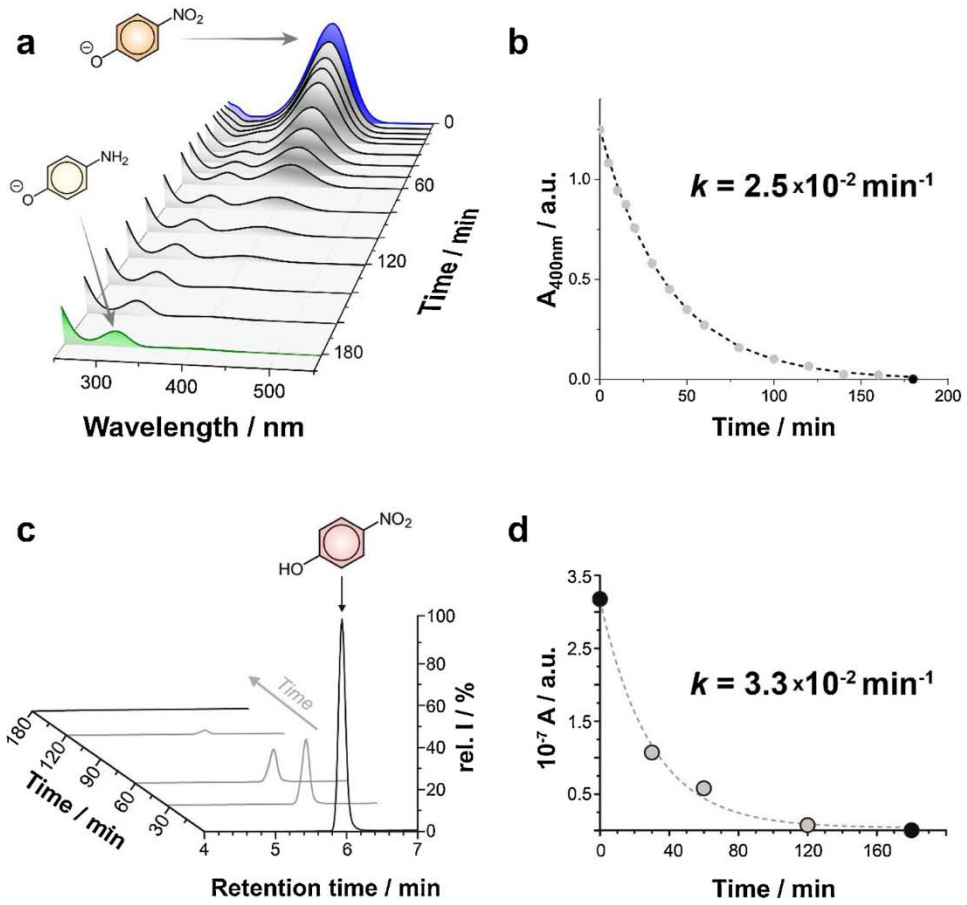

Fig. 5. (a) Time-dependent UV–vis spectra and (b) the corresponding kinetic rate and (c) HPLC chromatograms showing the evolution of the peak corresponding to 4-nitrophenol (t_R = 5.8 min) over time and (d) the corresponding kinetic rate for the 4-nitrophenol electrocatalyzed reduction using Au porous micropillars at 25 °C.

the peak at 5.8 min, corresponding to 4-nitrophenol, over time (Fig. 5c).

According to the Langmuir–Hinshelwood (L-H) model, when the concentration of the reactant is low, a pseudo-first-order reaction can be used to determine the kinetics of the process. Therefore, the apparent rate constant normalized by mass of gold or surface area (k in Table 2) was calculated by fitting a mono-exponential decay function to the data (absorbance at λ_{max} versus *t* for UV–vis spectroscopy or integrated area versus *t* for HPLC). Note that the kinetics of the electroreduction of 4-nitrophenol using porous Au micropillars was approximately 23 times greater than that with Au bare electrodes. A comparable enhancement is to be found through roughness factors since its value for porous Au micropillars was approximately 25 times greater than that of Au bare electrodes, which evidences that the electroreduction rate was proportional to the accessible surface area. That trend was confirmed by mass-normalized kinetic constants (i.e., the ratio of the rate constant *k* to the weight of the Au catalyst in each electrode). Thus, the reaction rate constants per unit mass were calculated to be 0.7 and 26 $min^{-1} g^{-1}$ for the reduction on the bare Au and porous Au micropillar electrodes, respectively. However, the kinetic constant normalized by real surface area was identical for bare Au and porous Au micropillar electrodes hence indicating that the surface

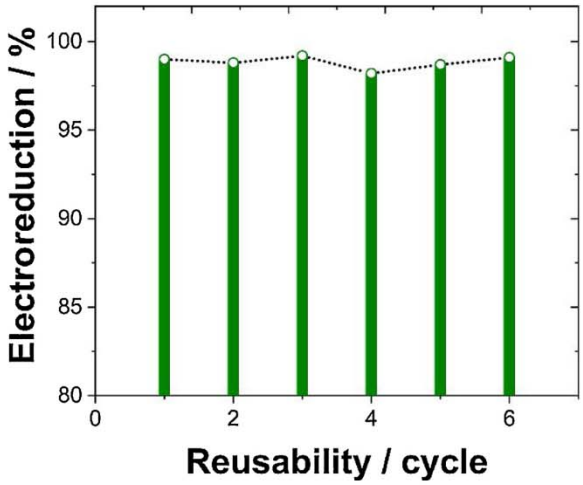

Fig. 6. Electroreduction efficiency of porous Au micropillars during 6 consecutive recycling cycles at -0.4 V versus Ag/AgCl/KCl (3 M)/Na_2SO_4 (0.5 M).

Table 2
Apparent kinetic constants for 4-nitrophenol electroreduction at T = 25 °C.

Electrode	k / min^{-1}		k / $min^{-1} cm^{-2}$		k / $min^{-1} g^{-1}$	
	UV–vis spectroscopy	HPLC	UV–vis spectroscopy	HPLC	UV–vis spectroscopy	HPLC
Au bare	1.1×10^{-3}	–	5×10^{-4}	–	0.7	–
Porous Au micropillars	2.5×10^{-2}	3.3×10^{-2}	5×10^{-4}	6×10^{-4}	26	34

reactivity was essentially the same for both electrodes despite dissimilar textures.

In an extended analysis of the potential of porous Au micropillar electrodes, their electroreduction yield during six cycles was measured (Fig. 6). The surface morphology (Fig. S5) and infrared spectra (Fig. S6) of porous Au micropillars were also examined after their reuse. Among the results, the activity, morphology, and surface functionalization exhibited no significant changes after the six cycles of reuse, which revealed their excellent stability as well as the absence of deactivation through poisoning during the electrocatalytic and reuse processes.

The electroreduction of 4-nitrophenol was thus shown to be an efficient and environmentally friendly method for the synthesis of 4-aminophenol since the use of potential dangerous and toxic redox agents was substituted with an electric current, while both high yields and high chemoselectivity were achieved.

4. Conclusions

The study presented here aims for the development of highly active and stable micro-architectured Au electrodes for the rapid and green conversion at room temperature of 4-nitrophenol into 4-aminophenol by a dual-template method utilizing SU-8 molds and colloidal crystal lithography through the galvanostatic electrodeposition technique. The major findings of this work can be summarized as follows:

- A simple, green, and scalable multi-step process for the electrosynthesis of architectured porous Au micropillar array electrodes was developed. The process was based on the use of a dual template method combined with galvanostatic electrodeposition of Au. Note that the technological process described in this work can be easily implemented at an industrial level, consequently extending it to other possible applications in different fields.
- The electrodeposition allowed the fabrication of well-defined macroporous Au micropillars, forming an accessible 3D porous network with high specific surface areas ($55.2\,m^2\,g^{-1}$) and high roughness factor (70.5).
- The high accessible surface area aforementioned was found to be closely linked to the remarkably high catalytic performance exhibited by architectured Au-based microelectrodes. The high versatility of colloidal crystal templating combined with electrodeposition opens up the way to producing electrocatalysts and sensors, among other applications, with enhanced effective area.
- A green and environmentally friendly pathway based on the electroreduction of 4-nitrophenol has been proposed for the electrosynthesis of 4-aminophenol and under possible convenience for the decontamination of wastewater. Importantly, the experimental conditions investigated in this study offered both excellent conversion yields (approximately 100 %) and chemoselectivity (no other byproducts were detected) while avoiding toxic reducing agents.
- The porous Au micropillars revealed that the yield, chemoselectivity, and catalytic performance were retained during several cycles, thus confirming that the structure retains its excellent stability as well as the absence of deactivation over multiple electrocatalytic processes.

CRediT authorship contribution statement

Maxime Tranchant: Conceptualization, Data curation, Formal analysis, Investigation, Methodology, Writing - original draft. **Albert Serrà:** Conceptualization, Methodology, Investigation, Formal analysis, Validation, Writing - original draft, Writing - review & editing. **Christopher Gunderson:** Conceptualization, Methodology, Investigation, Formal analysis, Validation, Writing - original draft, Writing - review & editing. **Enrico Bertero:** Investigation, Methodology. **Jaume García-Amorós:** Conceptualization, Methodology, Investigation, Formal analysis, Validation, Writing - review & editing. **Elvira Gómez:** Conceptualization, Validation, Supervision, Writing - review & editing, Funding acquisition. **Johann Michler:** Validation, Supervision, Writing - review & editing, Funding acquisition. **Laetitia Philippe:** Conceptualization, Validation, Supervision, Writing - review & editing, Funding acquisition.

Declaration of Competing Interest

The authors declare that they have no known competing financial interests or personal relationships that could have appeared to influence the work reported in this paper.

Acknowledgements

This work was partially supported by the Metrohm foundation. Partial funding from the TEC2017-85059-C3-2-R project (co-financed by the *Fondo Europeo de Desarrollo Regional, FEDER*) from the Spanish *Ministerio de Economía y Competitividad* (MINECO) is also acknowledged. Albert Serrà would like to acknowledge funding from the EMPAPOSTDOCS-II program. The EMPAPOSTDOCS-II programme has received funding from the European Union's Horizon 2020 research and innovation programme under the Marie Skłodowska-Curie grant agreement number 754364.

Appendix A. Supplementary data

Supplementary material related to this article can be found, in the online version, at doi:https://doi.org/10.1016/j.apcata.2020.117698.

References

[1] S.C. Mitchell, R.H. Waring, Aminophenols, Ullmann's Encyclopedia of Industrial Chemistry, Wiley-VCH, 2002.
[2] C.V. Rode, M.J. Vaidya, R.V. Chaudhari, Org. Process Res. Dev. 3 (1999) 465–470, https://doi.org/10.1021/op990040r.
[3] J.F. Corbett, Dyes Pigm. 41 (1999) 127–136, https://doi.org/10.1016/s0143-7208(98)00075-8.
[4] E. Friderichs, T. Christoph, H. Buschmann, Ullmann's Encyclopedia of Industrial Chemistry, Wiley-VCH, 2007.
[5] World Health Organization. World Health Organization model list of essential medicines: 21st list 2019. World Health Organization.
[6] J.O. Otutu, D. Okoro, E.K. Ossai, J. App. Sci. 8 (2008) 334–339.
[7] J. Zeng, Q. Zhang, J. Chen, Y. Xia, Nano Lett. 10 (2010) 30–35, https://doi.org/10.1021/nl903062e.
[8] P. Hervés, M. Pérez-Lorenzo, L.M. Liz-Marzán, J. Dzubiella, Y. Lu, M. Ballauff, Chem. Soc. Rev. 41 (2012) 5577–5587, https://doi.org/10.1039/c2cs35029g.
[9] M. Ruan, P. Song, J. Liu, E. Li, W. Xu, J. Phys. Chem. C. 121 (2017) 25882–25887, https://doi.org/10.1021/acs.jpcc.7b08787.
[10] S.K. Tanielyan, J.J. Nair, N. Marin, G. Alvez, R.J. McNair, D. Wang, R.L. Augustine, Org. Process Res. Dev. 11 (2007) 681–688, https://doi.org/10.1021/op700049p.
[11] C.V. Rode, M.J. Vaidya, R.V. Chaudhari, Org. Process Res. Dev. 3 (1999) 465–470, https://doi.org/10.1021/op990040r.
[12] C. Wang, L. Salmon, Q. Li, M.E. Igartua, S. Moya, R. Ciganda, J. Ruiz, D. Astruc, Inorg. Chem. 55 (2016) 6776–6780, https://doi.org/10.1021/acs.inorgchem.6b01092.
[13] S. Dutta, S. Sarkar, C. Ray, A. Roy, R. Sahoo, T. Pal, ACS Appl. Mater. Interfaces 6 (2014) 9134–9143, https://doi.org/10.1021/am503251r.
[14] J.C. Siu, N. Fu, S. Lin, Acc. Chem. Res. (2020), https://doi.org/10.1021/acs.accounts.9b00529.
[15] D.E. Blanco, M.A. Modestino, Trends Analyt. Chem. 1 (2019) 8–10, https://doi.org/10.1016/j.trechm.2019.01.001.
[16] F. Harnisch, U. Schröder, ChemElectroChem. 6 (2019) 4126–4133, https://doi.org/10.1002/celc.201900456.
[17] R. Francke, R.D. Little, Chem. Soc. Rev. 43 (2014) 2492–2521, https://doi.org/10.1039/c3cs60464k.
[18] N.H. Yeh, Y. Zhu, K.D. Moeller, ChemElectroChem. 6 (2019) 4134–4143, https://doi.org/10.1002/celc.201900851.
[19] G. Hilt, ChemElectroChem. 7 (2020) 395–405, https://doi.org/10.1002/celc.201901799.
[20] United States Environmental Protection Agency, Health and Environmental Effect Profiles, (1980).
[21] United States Environmental Protection Agency, Health Effects Assessment for Nitrophenols, (1987).
[22] G. Marcì, V. Augugliaro, M.J. López-Muñoz, C. Martín, L. Palmisano, V. Rives, M. Schiavello, R.J.D. Tilley, A.M. Venezia, J. Phys. Chem. B 105 (2001) 1033–1040, https://doi.org/10.1021/jp003173j.

[23] A. Serrà, Y. Zhang, B. Sepúlveda, E. Gómez, J. Nogués, J. Michler, L. Philippe, Water Res. 169 (2020), https://doi.org/10.1016/j.watres.2019.115210.
[24] A. Serrà, Y. Zhang, B. Sepúlveda, E. Gómez, J. Nogués, J. Michler, L. Philippe, Appl. Catal. B Environ. 248 (2019) 129–146, https://doi.org/10.1016/j.apcatb.2019.02.017.
[25] K.M. Parida, S.S. Dash, D.P. Das, J. Colloid Interface Sci. 298 (2006) 787–793, https://doi.org/10.1016/j.jcis.2005.12.053.
[26] J. Li, D. Kuang, Y. Feng, F. Zhang, Z. Xu, M. Liu, J. Hazard. Mater. 201–202 (2012) 250–259, https://doi.org/10.1016/j.jhazmat.2011.11.076.
[27] Z. Liu, J. Du, C. Qiu, L. Huang, H. Ma, D. Shen, Y. Ding, Electrochem. commun. 11 (2009) 1365–1368, https://doi.org/10.1016/j.elecom.2009.05.004.
[28] S. Lupu, C. Lete, M. Marin, N. Totir, P.C. Balaure, Electrochim. Acta 54 (2009) 1932–1938, https://doi.org/10.1016/j.electacta.2008.07.051.
[29] E.A. Hutton, B. Ogorevc, M.R. Smyth, Electroanalysis. 16 (2004) 1616–1621, https://doi.org/10.1002/elan.200402979.
[30] N.S. Lawrence, M. Pagels, A. Meredith, T.G.J. Jones, C.E. Hall, C.S.J. Pickles, H.P. Godfried, C.E. Banks, R.G. Compton, L. Jiang, Talanta 69 (2006) 829–834, https://doi.org/10.1016/j.talanta.2005.11.020.
[31] P. Cañizares, J. Lobato, R. Paz, M.A. Rodrigo, C. Sáez, Water Res. 39 (2005) 2687–2703, https://doi.org/10.1016/j.watres.2005.04.042.
[32] P. Cañizares, C. Sáez, J. Lobato, M.A. Rodrigo, Ind. Eng. Chem. Res. 43 (2004) 1944–1951, https://doi.org/10.1021/ie034025t.
[33] H. Míguez, F. Meseguer, C. López, A. Mifsud, J.S. Moya, L. Vázquez, Langmuir. 13 (1997) 6009–6011, https://doi.org/10.1021/la970589o.
[34] W.L. Vos, M. Megens, C.M. Van Kats, P. Bösecke, Langmuir. 13 (1997) 6004–6008, https://doi.org/10.1021/la970423n.
[35] T. Watanabe, Nano-plating, Microstructure Control Theory of Plated Film and Data Base of Plated Film Microstructure, Elsevier, 2004.
[36] A. Stein, R.C. Schroden, Curr. Opin. Solid State Mater. Sci. 5 (2001) 553–564, https://doi.org/10.1016/S1359-0286(01)00022-5.
[37] N.D. Denkov, O.D. Velev, P.A. Kralchevsky, I.B. Ivanov, Langmuir. 8 (1992) 3183–3190, https://doi.org/10.1021/la00048a054.
[38] R. Feng, R.J. Farris, J. Micromech. Microeng. 13 (2003) 80–88, https://doi.org/10.1088/0960-1317/13/1/312.
[39] Y. Song, C.S.S.R. Kumar, J. Hormes, J. Micromech. Microeng. 14 (2004) 932–940, https://doi.org/10.1088/0960-1317/14/7/013.
[40] M. Mieszala, Micro-mechanics of 3D Architectured Metals Synthesized by Electrodeposition, PhD thesis (2018).
[41] A. Serrà, N. Gimeno, E. Gómez, M. Mora, M.L. Sagristá, E. Vallés, Adv. Funct. Mater. 26 (2016) 6601–6611, https://doi.org/10.1002/adfm.201601473.
[42] S. Trasatti, O.A. Petrii, J. Electroanal. Chem. 321 (1993) 353–376.
[43] Y.P. Sun, W.L. Xu, K. Scott, Electrochim. Acta 38 (1993) 1753–1759, https://doi.org/10.1016/0013-4686(93)85073-8.
[44] A. Serrà, X. Alcobé, J. Sort, J. Nogués, E. Vallés, J. Mater. Chem. A 4 (2016) 15676–15687, https://doi.org/10.1039/c6ta07149j.
[45] H. Houcini, F. Laghrib, M. Bakasse, S. Lahrich, M.A. El Mhammedi, Int. J. Environ. Anal. Chem. 00 (2019) 1–12, https://doi.org/10.1080/03067319.2019.1655558.
[46] L. Qiang Luo, X. Lian Zou, Y. Ping Ding, Q. Sheng Wu, Sensors Actuators, B Chem. 135 (2008) 61–65, https://doi.org/10.1016/j.snb.2008.07.019.
[47] M.A. El Mhammedi, M. Achak, M. Bakasse, A. Chtaini, J. Hazard. Mater. 163 (2009) 323–328, https://doi.org/10.1016/j.jhazmat.2008.06.126.
[48] A. Serrà, R. Artal, M. Pozo, J. Garcia-Amorós, E. Gómez, Catalysts 10 (2020) 458, https://doi.org/10.3390/catal10040458.
[49] Z. Liu, J. Du, C. Qiu, L. Huang, H. Ma, D. Shen, Y. Ding, Electrochem. commun. 11 (2009) 1365–1368, https://doi.org/10.1016/j.elecom.2009.05.004.
[50] Y. Sang, B. Wang, Q. Wang, G. Zhao, P. Guo, Sci. Rep. 4 (2014) 1–6, https://doi.org/10.1038/srep06321.
[51] C.V. Rode, M.J. Vaidya, R.V. Chaudhari, Org. Process Res. Dev. 3 (1999) 465–470, https://doi.org/10.1021/op990040r.
[52] G. Greber, Brian S. Furniss, Antony J. Hannaford, Peter W.G. Smith, R. Austin (Eds.), Vogel'S Textbook of Practical Organic Chemistry, 5th ed., Tatchell, John Wiley & Sons, New York, 1991revised by.
[53] J. March, Advanced Organic Chemistry, 3rd ed., Wiley, New York, 1984.